

Characterization of the Strain Localization in a Porous Rock in Plane Strain Condition Using a New True-Triaxial Apparatus

P. Bésuelle and S.A. Hall

Abstract We present here first results obtained in a new true-triaxial apparatus that allows observation of the rock specimen under loading (up to a confining pressure equal to 100 MPa). The three principal stresses are independent, however the intermediate stress can also be controlled in order to impose a plane strain condition. Observation of a specimen under load is possible as one surface of the prismatic specimen, is in contact with a hard transparent window. Therefore the evolution of the strain field in the sample can be measured by digital image correlation (DIC) of photographs taken of this surface. We show some results on the evolution of the pattern in the post-localization regime in clay rock specimens.

Keywords Failure • Strain localization • Clay rocks • True-triaxial apparatus • Digital image correlation

1 Introduction

Failure by strain localization is commonly observed in geomaterials. In a previous workshop (IWBI Minneapolis St Paul, 2002), we presented an experimental characterization of strain localization in a porous sandstone (Bésuelle et al. 2000). This study was performed with classical axisymmetric triaxial compression tests. The effect of the confining pressure was observed on several aspects: onset of localization; pattern of localization; porosity evolution inside the localized bands. Complex patterns of localization were observed at high confining pressure in the transition between the brittle and ductile regimes, showing several deformation

P. Bésuelle (✉) · S.A. Hall
CNRS – UJF – Grenoble INP, Laboratoire 3SR, BP53, 38041 Grenoble Cedex 9, France
e-mail: Pierre.Besuelle@hmg.inpg.fr

bands in the specimens. However the history (time evolution) of the localization was not accessible because the observations were post-mortem.

Measurements of strain fields and their evolution in time are particularly useful to study strain localization (initiation of deformation bands) and post-localization regimes. Such tools have been developed for soils (e.g., sand specimens in plane strain conditions [Desrues and Viggiani 2004](#) or in triaxial conditions using X-ray tomography [Hall et al. 2010](#)). Similar developments for rocks are still difficult, especially because the pertinent confining pressure to reproduce in-situ stresses and material stiffnesses are higher than for soils; only a very few devices exist (e.g., [Takemura et al. 2004](#)).

We present here first results obtained in a new true-triaxial apparatus that allows observation of rock specimens under loading. Whilst several triaxial apparatuses exist that allow the application of three different principal stresses, they do not allow observation of specimens under load and such analysis is only possible post-mortem (e.g., [Mogi 1967](#); [Atkinson and Ko 1973](#); [Michelis 1985](#); [Wawersik et al. 1997](#); [Haimson and Chang 2000](#); [King 2002](#); [Naumann et al. 2007](#) and [Popp and Salzer 2007](#)). Furthermore, in this new device, as for biaxial apparatuses (e.g., [Ord et al. 1991](#) and [Labuz et al. 1996](#)), failure surfaces can develop and propagate in a sample in an unrestricted manner; this can be under true-triaxial or plane-strain (biaxial) conditions as, if required, the intermediate stress can be controlled (with active control) to impose a plane strain condition during a test. The observation of a specimen under load is possible as one surface of the prismatic specimen, which is orthogonal to the plane strain direction, is in contact with a hard transparent window. The deformation of this surface should be representative of the deformation in the whole specimen (due to the plane-strain condition), up to and beyond strain localization. Therefore the evolution of the strain field in a sample can be measured by digital image correlation (DIC) of photographs taken of this surface.

The next section describes briefly the new apparatus. We present in a third section preliminary results obtained with a porous clay rock, focusing on strain localisation and crack initiation.

2 Description of the True Triaxial Cell

The true-triaxial apparatus has been developed in Laboratoire 3SR (Grenoble) with the aim to characterize the initiation of localization and the post-localization regime in rocks. With this device three independent stresses can be applied in the three space directions on prismatic rock specimens, with the ability to visualise the specimen under load. The surfaces perpendicular to the major and intermediate stresses (compression) are in contact with rigid platens, which are moved by two perpendicular pistons, while the two surfaces perpendicular to the minor stress are free to deform because the stress is applied by a confining fluid (through a soft membrane). As deformation bands and cracks are generally parallel to the intermediate stress, the specimen has the freedom to deform and fail with no

kinematic constraints imposed on the formation of the failure zone. Moreover, one of the two surfaces perpendicular to the intermediate stress is in contact with a hard window to observe the specimen under load. The two pistons can be controlled in stress or displacement. The intermediate stress can be controlled such that there is no deformation in this direction, which allows application of plane strain loading. In such a case, the kinematics over the surface in contact with the window is representative of the kinematics in the whole specimen up to and beyond strain localization.

A simplified schema of the apparatus is presented in Fig. 1. The hydraulic axial piston (1) applies the axial loading on the specimen (2). This is self-compensated with respect to the confining pressure, i.e., it is in equilibrium whatever the confining pressure. The axial loading is controlled in displacement by an external displacement transducer linked to a pressure generator that adapts the pressure applied to the top of the piston to keep a constant displacement rate. The axial piston moves inside a floating axial frame (3), when the piston moves down, the frame and the bottom loading cap move up by about the same value. In such a way, if the specimen deforms homogeneously, the middle of the specimen does not move (or only very slightly). The weight of the floating frame is compensated by an external air piston.

The horizontal piston (4) applies the intermediate stress. This is also self-compensated with respect to the confining pressure inside the confining chamber (5). The piston can be controlled in displacement by the internal displacement transducers (6). One possible mode of operation is to adapt the pressure sent by its generator pressure to keep a zero displacement, i.e., a plane strain condition on the specimen, although all other controls in displacement or stress are possible. The surface of the specimen, opposed to the horizontal piston, is in contact with a thick, transparent sapphire window. This surface can be observed and photographs of the surface can be taken. For a symmetry of the contact, the surface on the side of the horizontal piston is in contact with a thin sapphire platen, to have the same boundaries conditions.

The minor stress is applied by the confining fluid on the two lateral surfaces of the specimen. The specimen is separated from the fluid by a silicone membrane. The membrane wraps around both the specimen and the four loading caps. In such a way, there is a direct contact between the specimen and the window. Note that in the axial direction, a special device of wedges between the specimen and the loading caps ensures that they have the same thickness as the specimen in the direction of intermediate stress. If a compression or extension of specimen in this direction occurs, the set of wedges automatically follow this change. This avoids an extrusion of the membrane during the deformation of the specimen.

A set a three pressure generators (syringe pumps with electronic control) is associated to the apparatus, to apply the loading in the three space directions. Further development is a control of the bottom and top pore pressure inside the specimen to impose a fluid flux. Note also that numerous electrical connectors in the cell allow to put several internal transducers, e.g., for acoustic emissions measurement.

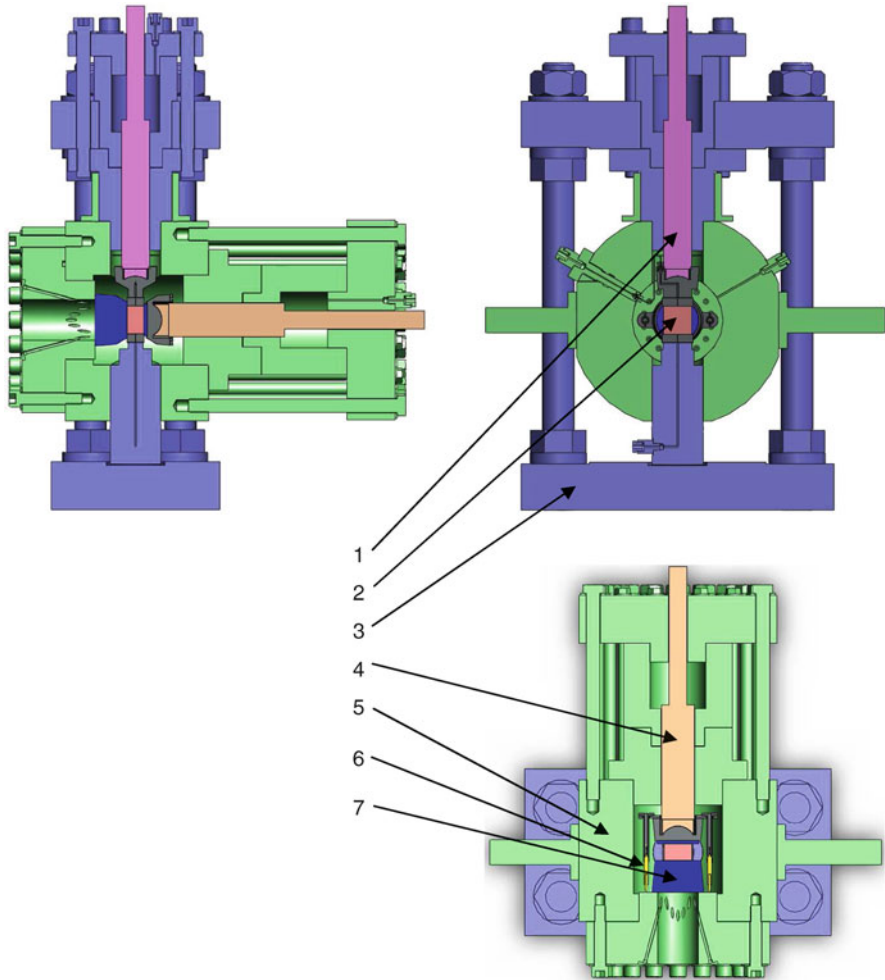


Fig. 1 Scheme of the true triaxial cell with an observation window: (1) axial piston, (2) specimen, (3) floating axial frame, (4) horizontal piston, (5) confining chamber and fixed frame, (6) internal displacement transducers, (7) sapphire window

The surface of the specimen is illuminated through the sapphire window by light from a set of LEDs focussed onto the sample surface through optical fibers; this provides a good and homogenous luminosity to take photographs. Photographs of the visible surface of the specimen were taken throughout the loading with a high resolution camera (providing images of $6,080 \times 4,044$ pixels). DIC analysis can thus be carried out on the resultant images to yield displacement and strain fields over the observed surface; for details on the DIC procedure see [Hall et al. \(2000\)](#). However, it is important to note that for the DIC, it is necessary to have a pattern over the surface of the sample that varies such that different parts of the surface can be

uniquely distinguished. Depending on the test specimen, this pattern can be natural (as with some sandstones for example) or artificial (in this case it was necessary to add this pattern as discussed later).

The size of the specimen is 50 mm in the axial direction, 30 mm in the direction of intermediate stress, and 25 or 50 mm in the direction of minor stress, which corresponds to slenderness ratios (the ratio of the height to the width) of two and one, respectively. The capacity of the cell for confining pressure is 100 MPa, the axial piston can apply a force of 500 kN and the horizontal piston a force of 700 kN, which correspond to a differential stress with respect to the confining pressure of 670 and 530 MPa, respectively, for a specimen with a slenderness ratio of two, and half that for a 50 mm width specimen.

3 Selected Results

We present here a test that has been performed on a clay rock specimen, the Callovo-Oxfordian argillite, from the underground research laboratory (URL) at Bure (Eastern France) at approximately 500 m below the ground surface. It is a sedimentary rock composed of particles of calcite and quartz in a clay matrix (Lenoir et al. 2007). The specimen has been prepared with a diamond wire saw and then polished with a fine sandpaper. The surface of the specimen in contact with the window of the triaxial apparatus has been painted with a thin layer of white ink and then a speckle of black ink, using an airbrush. The size of pixels in the photographs correspond to about $10\ \mu\text{m}$ on the sample surface. The test has been performed with an initial isotropic loading to 2 MPa and then an axial loading in plane strain conditions with a displacement rate of $1.25\ \mu\text{m}\cdot\text{s}^{-1}$, i.e., a strain rate of $2.5\ 10^{-5}\ \text{s}^{-1}$.

Figure 2 shows the evolution of the differential stress (major stress minus minor stress) with respect to the axial strain (specimen shortening divided by its initial height). A zoom of the full curve (left) is presented (right) for the period when the analyzed photographs were taken. The beginning of the curve at left is quite linear, followed by a small curvature and a first stress peak at 0.02 axial strain, followed by a strong stress drop. Then a slow stress increase is observed, followed by a second stress drop at 0.42 axial strain. After, the stress is quite constant. The two stress drops are associated with major failure by faulting in the specimen. The crack that appeared during the second drop is conjugate to the first crack set, which appeared at the first drop. We focus later on the strain localization at first stress peak.

Figure 3 presents the fields of a few axial displacement increments before and after the stress peak. The specimen deformation during increment 3,388–3,390 seems quite homogeneous, and the displacements are primarily vertical.¹ The increment 3,392–3,393 shows a loss of the homogeneity with a gradient of

¹The top displacement is approximately the same but opposite to the bottom displacement, due to the conception of the apparatus. The middle of the specimen does not move in the axial direction.

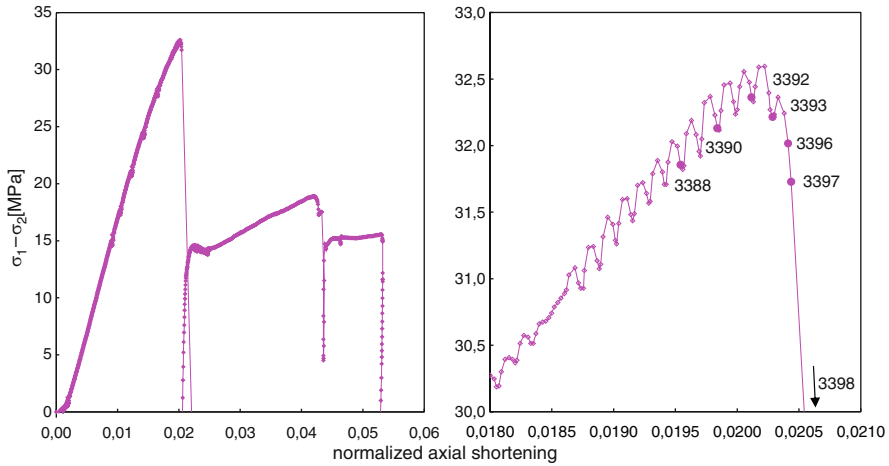


Fig. 2 Evolution of the differential stress (major stress minus minor stress) versus axial strain. At right, detail of the full curve at left, close to the stress peak. Numbers correspond to the photographs (The small oscillations of the right curve have been induced by an imperfect regulation of the axial piston pressure generator)

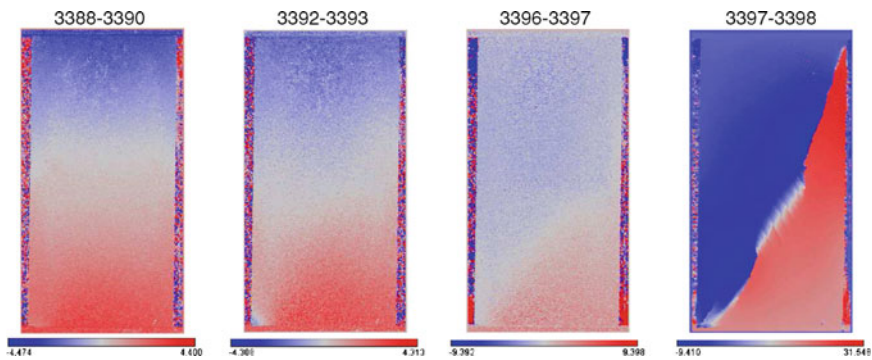


Fig. 3 Fields of axial displacement increments close to the stress peak. Couples of numbers on the top of each picture correspond to the photographs numbers used for the DIC. The color scales are expressed in term of pixel size (about 10 μm)

displacement oriented along an inclined line from the bottom left to the top right of the specimen. This corresponds to an incipient strain localization arriving at the stress peak. A shear band is observed in further increments up to photograph 3,397. During increment 3,397–3,398, a strong discontinuity is observed in the displacement field, which corresponds to a crack initiation in the place of the previous shear band. The strain field of this increment is shown in Fig. 4, where the maximum shear strain and volume strain are plotted. A major crack crosses the specimen from the bottom left to the top right. In the central zone of the specimen, there is a set of small conjugate cracks, showing two, quite close, preferential

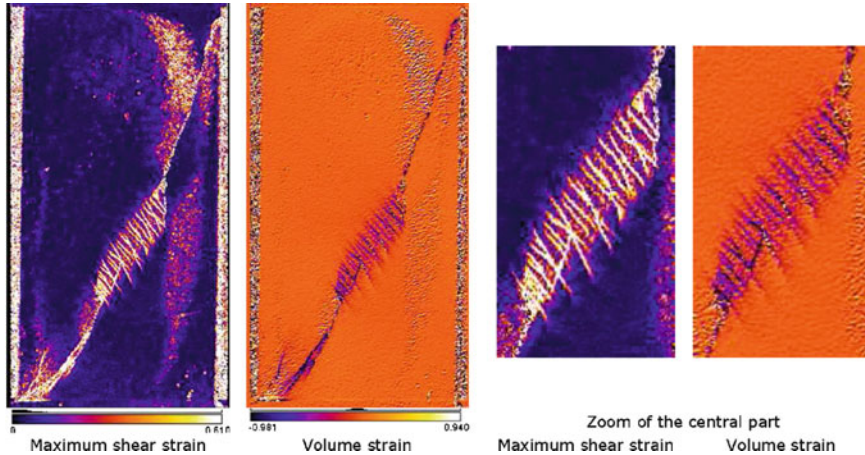


Fig. 4 Fields of shear and volume strain during increment 3,397–3,398

orientations. These small cracks are arranged inside an elongated zone parallel to the major crack. In most of cases, the major and small crack initiation is associated with a compaction combined with shear sliding. The sub-vertical zone of concentration of the shear strain on the right of the specimen is in fact an artefact of the measure due to a change of luminosity of the surface of the specimen in contact with the window (probably a consequence of an initial small default of planarity of the specimen).

A post-mortem analysis of the specimen using our X-ray CT apparatus shows the 3D network of cracks. The major cracks cross the specimen roughly parallel to the direction of intermediate stress, confirming a 2D mechanism of deformation in the specimen. The central zone of conjugate small cracks extends about half of the way into the specimen in the intermediate stress direction, which confirms that the conjugated cracks are not a surface effect but bulk mechanism of deformation.

4 Conclusions

The ability to characterize localized failure in rocks and, in particular, to follow the strain field evolution inside rock specimens during loading using a new true-triaxial apparatus has been demonstrated. Displacement and strain fields results, using DIC, from a plane-strain loading test on a clay rock have been presented, which reveal a complex pattern of localization at failure. Furthermore the evolution of the deformation has been followed from an initially homogeneous deformation through the development of a shear band and subsequent initiation of a set cracks resulting in major faults and small conjugate cracks arranged inside a band parallel to the major fault. Further experiments will focus on the effect of confinement on the processes of failure and localization and also on reproducibility in similar conditions.

Acknowledgements The authors thank the French radioactive waste management agency (ANDRA) who provides the clay rock from its URL at Bure. The development of the true triaxial apparatus has been supported by the 'ACI jeunes chercheurs JC8029' from the French government, by the national research group 'GDR FORPRO' from CNRS and by ANDRA.

References

- R.H. Atkinson, H.-Y. Ko, A fluid cushion, multiaxial cell for testing rock specimens. *Int. J. Rock Mech. Min. Sci. Geomech. Abstr.* **10**, 351–361 (1973)
- P. Bésuelle, J. Desrues, S. Raynaud, Experimental characterisation of the localisation phenomenon inside a Vosges sandstone in a triaxial cell. *Int. J. Rock Mech. Min. Sci.* **37**, 1223–1237 (2000)
- J. Desrues, G. Viggiani, Strain localization in sand: an overview of the experimental results obtained in Grenoble using stereophotogrammetry. *Int. J. Numer. Anal. Methods Geomech.* **28**, 279–321 (2004)
- B. Haimson, C. Chang, A new true triaxial cell for testing mechanical properties of rock, and its use to determine rock strength and deformability of Westerly granite. *Int. J. Rock Mech. Min. Sci.* **37**, 285–296 (2000)
- S.A. Hall, D. Muir Wood, E. Ibraim, G. Viggiani, Localised deformation patterning in 2D granular materials revealed by digital image correlation. *Granul. Matter* (2000). doi:10.1007/s10035-009-0155-1
- S.A. Hall, M. Bornert, J. Desrues, Y. Pannier, N. Lenoir, G. Viggiani, P. Bésuelle, Discrete and continuum analysis of localised deformation in sand using X-ray micro CT and volumetric digital image correlation. *Géotechnique* **60**, 315–322 (2010)
- M.S. King, Elastic wave propagation in and permeability for rocks with multiple parallel fracture. *Int. J. Rock Mech. Min. Sci.* **39**, 1033–1043 (2002)
- J.F. Labuz, S.-T. Dai, E. Papamichos, Plane-strain compression of rock-like materials. *Int. J. Rock Mech. Min. Sci. Geomech. Abstr.* **33**, 573–578 (1996)
- N. Lenoir, M. Bornert, J. Desrues, P. Bésuelle, G. Viggiani, Volumetric digital image correlation applied to X-ray microtomography images from triaxial compression tests on argillaceous rock. *Strain* **43**, 193–205 (2007)
- P. Michelis, A true triaxial cell for low and high pressure experiments. *Int. J. Rock Mech. Min. Sci. Geomech. Abstr.* **22**, 193–188 (1985)
- K. Mogi, Effect of the intermediate principal stress on rock failure. *J. Geophys. Res.* **72**, 5117–5131 (1967)
- M. Naumann, U. Hunsche, O. Schulze, Experimental investigations on anisotropy in dilatancy, failure and creep of Opalinus Clay. *Phys. Chem. Earth* **32**, 889–895 (2007)
- A. Ord, I. Vardoulakis, R. Kajewski, Shear band formation in Gosford sandstone. *Int. J. Rock Mech. Min. Sci. Geomech. Abstr.* **28**, 397–409 (1991)
- T. Popp, K. Salzer, Anisotropy of seismic and mechanical properties of Opalinus clay during triaxial deformation in a multi-anvil apparatus. *Phys. Chem. Earth* **32**, 879–888 (2007)
- T. Takemura, M. Oda, M. Takahashi, Microstructure observation in deformed geomaterials using microfocus X-ray computed tomography, in *X-ray CT for Geomaterials, GeoX2004*, ed. by J. Otani, Y. Obara (Balkema, Rotterdam, 2004)
- W.R. Wawersik, L.W. Carlson, D.J. Holcomb, R.J. Williams, New method for true-triaxial rock testing. *Int. J. Rock Mech. Min. Sci.* **34**, 330 (1997)